



# Environmental effects on forage and longline fishery performance for albacore (*Thunnus alalunga*) in the American Samoa Exclusive Economic Zone

RÉKA DOMOKOS\*

National Marine Fisheries Service, NOAA, Pacific Islands Fisheries Science Center, 2570 Dole Street, Honolulu, HI 96822-2396, USA

## ABSTRACT

The South Equatorial Counter Current (SECC) strongly influences the American Samoa Exclusive Economic Zone (EEZ) and changes strength on a seasonal and ENSO cycle. A strong SECC is associated with a predominantly anticyclonic eddy field as well as increased micronekton biomass and catch-per-unit-effort (CPUE) for albacore tuna, the economically important target species of the local longline fishery. A strong SECC carries chlorophyll *a*-rich waters from upwelling regions at the north coast of New Guinea towards the EEZ, most likely resulting in the observed increase in micronekton biomass, forage for albacore. Relatively stable anticyclonic eddies show a further increase in micronekton biomass, apparently advected from neighboring SECC waters. The presence of forage presumably concentrates albacore, thus resulting in the observed increase in CPUE. High shear regions of neither anticyclonic nor cyclonic eddies correlate with increased micronekton biomass. Areas characterized by South Equatorial Current (SEC) waters correspond to areas with the lowest micronekton biomass and the highest number of aggregative structures, which are most likely small pelagic fish shoals. Micronekton composition in SEC waters differs from that in the SECC. During El Niños, the seasonal signals at the north shore of New Guinea and in the SECC are exceptionally strong and correspond to higher albacore CPUE in the EEZ. My results suggest that the strength of upwelling and the resulting increase in chlorophyll *a* at New Guinea, as well as the Southern Oscillation

Index, could be used to predict the performance of the local longline fishery for albacore tuna in the American Samoa EEZ.

**Keywords:** active acoustics, albacore tuna, American Samoa Exclusive Economic Zone, anticyclonic eddies, catch-per-unit-effort, convergence, deep scattering layer, El Niño Southern Oscillation, longline fishery, mesoscale eddy, micronekton distribution, shallow scattering layer, South Equatorial Counter Current, South Equatorial Current, South-Western Pacific, subsurface zonal jet, water masses

## INTRODUCTION

Albacore tuna *Thunnus alalunga* is an economically important species in the South Pacific which supports several local fisheries, such as in American Samoa, Samoa, French Polynesia, Fiji, and Tonga. Combined catch rates from this region account for more than 50% of the total global albacore catch, with 20% of this landed by the American Samoa domestic longline fishery alone (Langley, 2006). The American Samoa longline fishery operates primarily in the American Samoa Exclusive Economic Zone (EEZ) targeting albacore and supplying a significant portion of canned albacore tuna for the US market (Domokos *et al.*, 2007). Note that the irregular shape of the EEZ is the result of the proximity of other countries in the vicinity of American Samoa, especially the nearby Samoan Islands to the west, as neighboring countries negotiate the borders of their EEZs. The longline fishery started operating in 1995 and then underwent rapid growth in 1999–2001 before stabilization of the fleet in 2002. Albacore catch and catch-per-unit-effort (CPUE) have undergone extreme fluctuations, with a peak in 2002, a steep decline in 2004, and a modest recovery in recent years. This raises questions about the extent of the impact of the fishery in comparison with other effects, such as changing oceanographic conditions in the region.

Fisheries performance for tuna and other top predators has been shown to depend on environmental

\*Correspondence. e-mail: reka.domokos@noaa.gov

Received 27 June 2008

Revised version accepted 21 July 2009

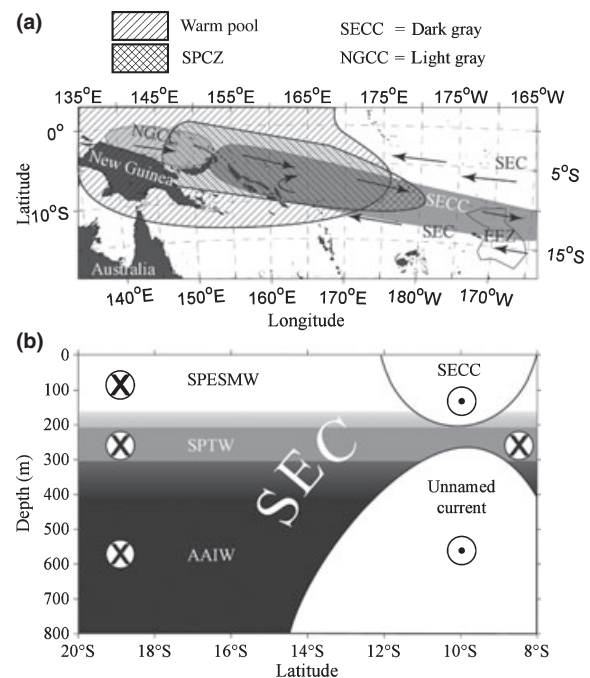
factors, as the environment can affect either catchability (e.g., Boggs, 1992; Bigelow *et al.*, 2002, 2006; Ward and Myers, 2005; Ménard *et al.*, 2007), fish abundance (e.g., Lehodey *et al.*, 1997, 1998; Lehodey, 2001; Polovina *et al.*, 2001), or both (e.g., Cushing, 1982; Walther *et al.*, 2002). Environmental factors, such as dissolved oxygen concentrations (DO) and temperature, can affect top predator abundance directly (e.g., Graham *et al.*, 1989; Bertrand *et al.*, 2002b) or indirectly through affecting the distribution and abundance of their prey. For example, cyclonic, upwelling eddies are thought to enhance growth of prey organisms as a result of enhanced primary productivity associated with their cores, whereas convergent regions, such as high-shear regions of eddy edges, can aggregate nearby organisms. Eddy edges have been found to have increased albacore CPUE, thought to be the result of higher concentrations of prey (e.g., Laurs and Lynn, 1977; Laurs *et al.*, 1984).

There has been only one oceanographic study of the pelagic habitat in the American Samoa EEZ and its effects on albacore CPUE. Domokos *et al.* (2007) showed the presence of seasonally varying mesoscale eddy activity in the American Samoa EEZ with a positive effect on albacore CPUE. For the 2-yr period of 2002–2003, albacore CPUE peaked from May to early July. During peak times, most albacore were caught at high-shear regions associated with eddy edges, consistent with observations in other regions (e.g., Laurs and Lynn, 1977; Laurs *et al.*, 1984).

However, Domokos *et al.* (2007) failed to find higher concentrations of micronekton, prey for albacore, at high-shear edges of cyclonic eddies in the EEZ during a 2-week observational period in 2004. While the lack of an effect of cyclonic eddies on micronekton biomass is in contrast to expectations (e.g., Wiebe and Joyce, 1992; Sassa *et al.*, 2002), it is consistent with some findings (e.g., Ménard *et al.*, 2005) and could be based on the fact that most micronektonic organisms exhibit a diel vertical migratory pattern and occupy depths below the influence of mesoscale eddies during the day. Further, most of our knowledge of the effects of eddies on micronekton comes from studies focused on frontal eddies associated with boundary currents (e.g., Wiebe and Joyce, 1992; Sassa *et al.*, 2002) or on eddies formed by the interaction of boundary currents with topography (Ménard *et al.*, 2005).

There are characteristic differences between frontal eddies and eddies in the American Samoa EEZ. Domokos *et al.* (2007) showed that eddies in the EEZ are mid-ocean eddies that define the seasonally modulating South Equatorial Counter Current (SECC). The SECC is a slow current confined to the

**Figure 1.** Schematic representation of the (a) horizontal current system over the South-western Pacific during boreal winter and (b) the vertical structure of the currents and water masses in the American Samoa Exclusive Economic Zone (EEZ; cross-section at  $\sim 169^\circ\text{W}$ ). Arrowheads and arrow-tails in (b) indicate eastward and westward flow, respectively. The American Samoa EEZ is located at the bottom right of the top panel ( $\sim 14^\circ\text{S}$   $169^\circ\text{W}$ ), marked as EEZ. SPCZ, South Pacific Convergence Zone; NGCC, North Guinea Coastal Current; SECC, South Equatorial Counter Current; SEC, South Equatorial Current; SPESMW, South Pacific Eastern Subtropical Mode Water; SPTW, South Pacific Tropical Water; AAIW, Antarctic Intermediate Water.



upper 175–200 m (Qu and Lindstrom, 2002) (Fig. 1), typically peaking in March and April (Qiu and Chen, 2004). Eddies are formed over the path of the SECC as a result of horizontal shear between the eastward flowing SECC and the westward flowing South Equatorial Current (SEC). As opposed to frontal cyclonic (divergent, ‘cold-core’) or anticyclonic (convergent, ‘warm-core’) eddies, mid-ocean eddies are formed from relatively homogeneous waters and do not have near-surface temperature signatures in the EEZ (Domokos *et al.*, 2007). These differences are expected to result in effects on the local micronekton community that are unlike those of frontal or boundary current eddies.

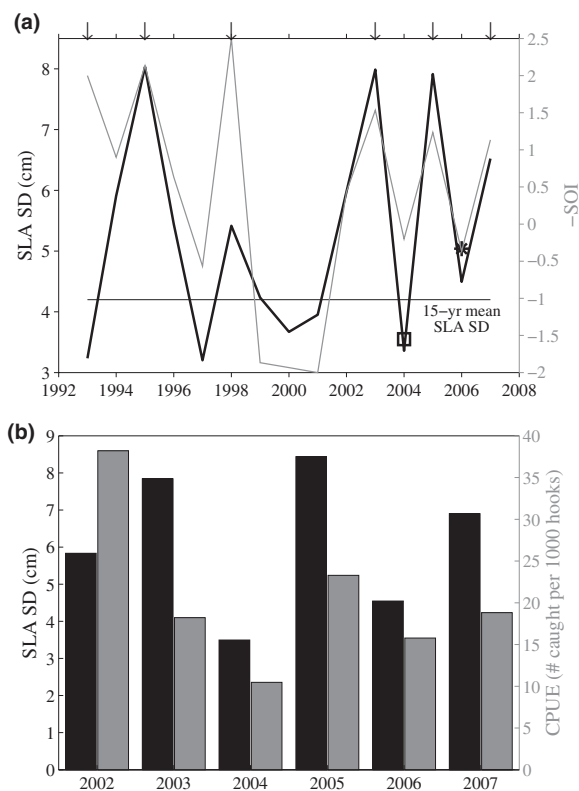
Although Domokos *et al.* (2007) did not find eddy effects on micronekton concentrations and/or distribution in the EEZ, all other evidence points to the fact

that high albacore CPUE is the result of higher concentrations of albacore in the presence of prey. Domokos *et al.* (2007) showed that in the American Samoa EEZ, variability in CPUE is not due to catchability issues. Further, the distribution of albacore is not a result of direct environmental effects; rather, it is associated with a permanent, thin layer of micronekton in the EEZ. These findings correspond to those from the neighboring French Polynesia showing that the distribution of albacore is driven by the presence of its prey (e.g., Josse *et al.*, 1998; Bertrand *et al.*, 1999, 2002a,b).

I hypothesize that the reason Domokos *et al.* (2007) failed to find increased micronekton biomass associated with eddy edges is due to a failure of the SECC to intensify during the March 2004 *in situ* observations. In the absence of the SECC, eddies were not associated with SECC waters and their activity (measured by the standard deviation of sea level anomaly, SLA SD; see Materials and methods) was one of the lowest during the past 15 yrs (Fig. 2a). The timing of the failure of the SECC and the absence of its eddies correspond to the timing of the lowest albacore CPUE on record (Fig. 2b), supporting the hypothesis that the absence of the SECC and its eddies resulted in relatively low micronekton concentrations, less albacore in the region, and the observed low in their CPUE.

Whereas the origin of the seasonal variability in the strength of the SECC is well understood, the reason for interannual variability, such as the 2004 event, is not known. I propose that anomalous wind stress and wind stress curl during El Niños and La Niñas over the South Pacific warm pool (e.g., Lukas and Lindström, 1991; Ridgway *et al.*, 1993; Holbrook and Bindoff, 1997), the origin of the SECC (Fig. 1a), result in changes in the strength of the SECC and the associated eddy activity, affecting albacore CPUE in the EEZ. Typically, seasonality in the wind stress curl drives an annual cycle in the strength of the Pacific subtropical gyre by spinning up the gyre in the latter part of the year and weakening circulation in the beginning of the year (Kessler and Gourdeau, 2007). Spatial patterns inherent in the wind stress curl are also responsible for breaking the South Equatorial Current (SEC) into several strong zonal jets as far east as 120°W (Kessler and Gourdeau, 2006). When gyre circulation is relatively low, mean westward flow is weak, and the SECC becomes stronger and moves east between two SEC jets (Fig. 1a). Li and Clarke (2007) showed that during El Niño (La Niña) events, increased (decreased) wind stress and positive (negative) wind stress curl anomaly result in positive (negative) sea level anomaly (SLA) in the warm pool,

**Figure 2.** Time series of standard deviation of sea level anomaly (SLA SD) with (a) the Southern Oscillation Index (SOI) and (b) albacore catch per unit effort (1000 caught per hook; CPUE) in the American Samoa EEZ. As negative values of SOI correspond to El Niño events,  $-SOI$  is plotted for display. Means are calculated over the peak 3-month periods for SLA SD (March–May) and CPUE (April–June), and for the 3-month period of the previous October–December for SOI, the peak of El Niño influence at the origin of the South Equatorial Counter Current. Arrows in (a) indicate the El Niño events, while the square and star represent the mean SLA SD for the period of the 2004 and 2006 observations, respectively. The horizontal line is the 15-yr mean.



especially along the track of the SECC (compare Fig. 1a and Li and Clarke's Fig 1). Positive (negative) SLA of the SECC during El Niños (La Niñas) suggests exceptionally strong (weak) eastward velocities of the SECC during these times.

The present study tests the hypothesis that the SECC and its associated eddy activity result in increased micronekton biomass in the American Samoa EEZ. This study also shows that interannual variability in the SECC is the result of the ENSO cycle. I show that SECC waters contain higher micronekton biomass than SEC waters. The increase in micronekton biomass are linked to seasonal upwelling at the north

coast of New Guinea and to the resulting increase in chlorophyll *a* (Chl *a*), which is carried east by the SECC. I argue that the high Chl *a* in SECC waters results in high micronekton biomass, which is carried by the intensified SECC into the EEZ. The increase in forage most likely attracts albacore into the region and results in the observed increase in albacore CPUE. I identify crucial environmental factors affecting albacore CPUE, which are essential for understanding CPUE variability for this economically important species.

## MATERIALS AND METHODS

To examine the effects of the SECC and its associated eddies on the physical and biological characteristics of the American Samoa EEZ, both *in situ* and remote sensing data were used. The influence of ENSO on the SECC was assessed from the Southern Oscillation Index (SOI), while fishery performance for albacore was obtained from the federal logbook records of the American Samoa longline fishery.

*In situ* data were collected on board the NOAA Ship *Oscar Elton Sette* between 15 February and 2 March 2006. Cruise tracks of the *Oscar Elton Sette* were divided into 11 sections for clarity (Table 1). The four panels of Fig. 3 depict the tracks and the corresponding weekly averages of SLA (see below), each map 3.5 days apart as the weekly SLA records overlap in time.

### Oceanographic characteristics

*In situ* hydrographic data down to 1000 m depth were collected via CTD casts every 15 feet along four sections of the cruise, marked by green lines on Fig. 3: through a relatively large, slow-moving, long-lived (1–2 months) anticyclonic eddy at the northwest

corner of the EEZ (the Northwest Eddy, top left panel); along a transect from the Northwest Eddy to the outside of the eddy (Transect 1, top right panel); along a transect in the southern half of the EEZ, away from anticyclonic eddies (Transect 2, bottom right panel); and along a transect traversing a short-lived (<2 weeks), weak anticyclonic eddy in the southern half of the EEZ (Transect 3, bottom left panel). All casts used a SeaBird SBE 9/11+ CTD system equipped with redundant temperature, conductivity, and dissolved oxygen sensors and a Seapoint fluorometer for *in vivo* chlorophyll (chlorophyll + phaeopigments) determination.

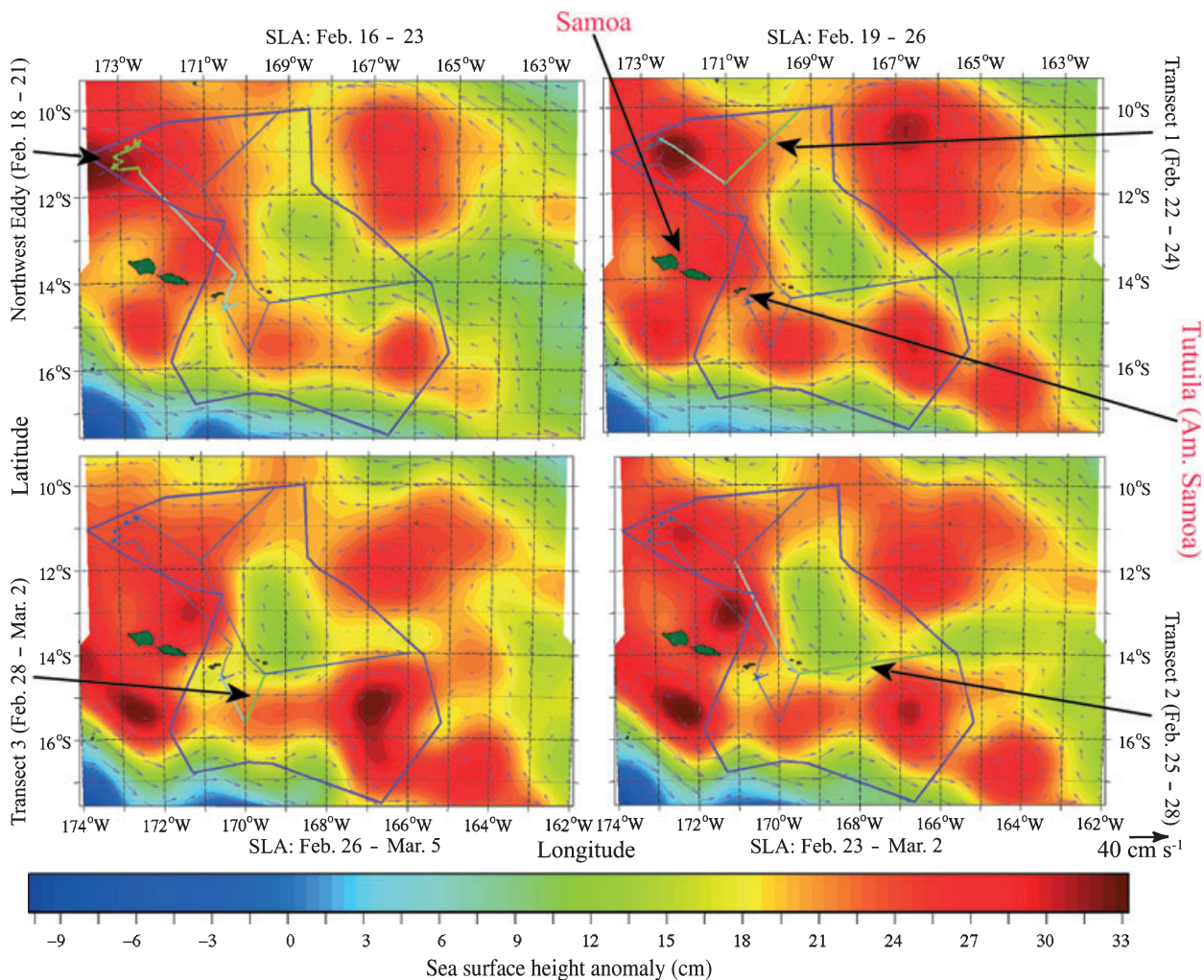
To obtain information on the currents in the region, *in situ* acoustic Doppler current profiles (ADCP) were collected continuously during the entire cruise (Fig. 3). The *Oscar Elton Sette* is equipped with a hull-mounted, RD Instruments ADCP system, operating at 75 kHz frequency. Raw zonal and meridional currents were processed using the CODAS software developed at the University of Hawaii at Manoa (see [http://currents.soest.hawaii.edu/docs/adcp\\_doc/index.html](http://currents.soest.hawaii.edu/docs/adcp_doc/index.html)). During processing, data were averaged into 20-m vertical and 2500-m horizontal bins, from the surface down to 700 m depth. Below 700 m, the signal-to-noise ratio became too low for quantitative analysis.

To characterize the strength of the SECC and the eddy fields in the American Samoa EEZ, a weekly SLA data product, mapped to a global  $0.3^\circ \times 0.3^\circ$  Mercator projection with orbit error reduction, was obtained from the SSALTO program of the Centre National d'etudes Spatiales, Romonville, St. Agne, France. At the time of the study, data were available from October 1992 to October 2007. These data are the AVISO TOPEX/POSEIDON altimetry from October 1992 to July 2002, after which JASON-1 was put into orbit, replacing TOPEX/POSEIDON and providing altimetry along the same track with similar resolution.

**Table 1.** Locations of the 11 sections of the cruise tracks. The 'panel' and 'color' column refer to the appearance of the section in Fig. 3. Boldface indicates the transects for which CTD data are available.

Transect name	Location	Panel	Color
Test Site	South of Tutuila, ~170°45'W, 14°15'S	upper left	light blue
Test to Northwest Eddy	~170°45'W, 14°15'S to 173°W, 11°S	upper left	light blue
<b>Northwest Eddy</b>	northwest EEZ, ~173°W, 11°S	upper left	green
Eddy to Transect 1	~173°W, 11°S to ~171°W, 12°S	upper right	light blue
<b>Transect 1 East</b>	or 'Transect 1', ~171°W, 12°S to 169°10'W, 10°S	upper right	green
Transect 1 West	same as Transect 1 East but going West	upper right	green
Transect 1 to Transect 2	~171°W, 12°S to 168°30'W, 14°30'S	lower right	light blue
<b>Transect 2 East</b>	or 'Transect 2', 169°30'W, 14°30'S to 166°W, 14°S	lower right	green
Transect 2 West	same as Transect 2 East but going West	lower right	green
<b>Transect 3 South</b>	or 'Transect 3', 169°30'W, 14°30'S to 170°W, 15°30'S	lower left	green
Transect 3 North	~170°W, 15°30'S to Tutuila (~170°45'W, 14°15'S)	lower left	light blue

**Figure 3.** Four consecutive weekly SLA maps, clockwise from top left, of the American Samoa EEZ with cruise tracks of the *Oscar Elton Sette*. Red line: boundary of the EEZ; green and light blue lines: cruise tracks corresponding in time to the SLA maps for tracks with and without CTD casts, respectively; dark blue line, cruise tracks outside the period of the SLA data. Arrows show the large-scale geostrophic current flow.



SLA is calculated as relative to the mean of the along-track TOPEX/POSEIDON sea level height then gridded to create a  $0.25^\circ \times 0.25^\circ$  SLA field. The strength of the SECC was assessed from its eddy activity, as the intensity of the SECC is reflected in its eddy kinetic energy (Qiu and Chen, 2004). The strength of eddy activity was calculated as the mean of SLA standard deviations (SD) over an area in the path of the SECC, defined by  $160\text{--}180^\circ\text{E}$ ,  $8\text{--}12^\circ\text{S}$ . Eddy activity in the American Samoa EEZ was obtained from the mean SLA SD over the area of the EEZ.

To obtain information on primary productivity in the SECC and SEC, monthly satellite surface Chl *a* data collected by the Sea-viewing Wide Field-of-view Sensor (SeaWiFS) were used. On board the

Seastar spacecraft, the SeaWiFS instrument began providing remotely-sensed Chl *a* estimates in September 1997. This data product is derived from discrete measured wavelength bands and is available with a 9-km pixel resolution on an equidistant cylindrical projection. For this study, the most recent version of the data (version 5.2) was obtained for the area depicted in Fig. 1a. This version, available from July 2007, has undergone numerous reprocessing to incorporate algorithm improvements, recalibrations, and corrections for drift and slight degradation of the sensors. At the time of analyses, data from this version were available from September 1997 to June 2007, providing a high-quality, nearly decade-long dataset.

To examine possible correlations between the occurrence of El Niños and the interannual variability in eddy activity and albacore CPUE in the EEZ, monthly SOI and official El Niño years were obtained from the Western Regional Climate Center from September 1991 to October 2007. This time period corresponds in time to the available satellite altimetry data product with a 12 to 0 month lag. Since SOI is the difference in sea surface pressure anomaly between Tahiti and Darwin (Tahiti – Darwin), SOI was multiplied by  $-1$  for El Niños to be indicated by positive values. To compare the level of weekly eddy activity to the SOIs, weekly mean SDs for the area of the EEZ were interpolated to obtain monthly SLA SD time series, which then could be compared directly to the monthly SOI.

#### *Longline fishery performance for albacore*

Data obtained from mandatory commercial longline fishery logbooks, collected since 1996, show that since 2002, the ‘post-expansion’ period for the fishery, the number and composition of the fleet, the locations of fishing, type of gear, number of sets and the number of hooks per set, have been relatively steady. Data only from this steady period were used to avoid any artifacts caused by changes in the fishery. CPUE (number caught per 1000 hooks) was calculated from the number of albacore caught and number of hooks over the area of the EEZ from January 2002 to October 2007, the extent of available records.

#### *Micronekton distribution*

To obtain information on the distribution and relative abundance of micronekton, relative micronekton density and biomass were estimated from *in situ* acoustic backscatter data collected continuously on board the *Oscar Elton Sette*. The ship is equipped with a hull-mounted Simrad EK60 split-beam echosounder system operating at 38-kHz and 120-kHz frequencies. Three months prior to the cruise, the system was calibrated using a 38.1-mm-diameter tungsten carbide sphere. Both transducers, with  $\sim 7^\circ$  beam-widths, were set to operate with 1024  $\mu$ s pulse lengths at 2 kW and 0.5 kW power for the 38-kHz and 120-kHz channels. The minimum threshold for the mean volume backscattering strengths ( $S_v$ ), a proxy for relative density (Simmonds and MacLennan, 2005), was set to  $-75$  dB to avoid backscatter from plankton and other smaller organisms. These settings gave approximate ranges of 1600 and 300 m for the 38-kHz and 120-kHz frequencies, with a 10-dB minimum for signal-to-noise ratio at the maximum depths. Data from the upper

15 m were discarded for being too close to the transducers for quantitative analysis. The dual frequency system with the above settings allowed for some relative scattering layer composition estimates in the upper 300 m, as organisms have distinct scattering properties at the two frequencies (e.g., Jech and Michaels, 2006; Kang *et al.*, 2002; Lawson *et al.*, 2008). The method of ‘dB differencing’, defined here as  $\delta S_v = 120 \times 38 \text{ kHz } S_v$ , can be used successfully to identify various types of micronekton and/or fish in acoustic data (e.g., Madureira *et al.*, 1993; Goss *et al.*, 2001; Simmonds and MacLennan, 2005; Ressler *et al.*, 2004; Lavery *et al.*, 2007).

Prior to processing, noisy pings and bubble dropouts were removed using ECHOVIEW<sup>®</sup> software (Myriax Ply Ltd, Hobart, Tasmania) and echograms were visually inspected to ensure the quality of data.  $S_v$  was integrated over deep bins 50 m long by 5 m deep down to 1000 and 300 m for the 38-kHz and 120-kHz frequencies, then converted to nautical area-scattering coefficients, NASC (e.g., Simmonds and MacLennan, 2005; MacLennan *et al.*, 2002), in units of  $\text{m}^2 \text{ nmi}^{-2}$  (nmi = nautical miles). NASC, the integral of relative density, can be used as a proxy for relative biomass assuming that the composition of the scattering layers and the resulting scattering properties of micronekton do not change significantly (e.g., Lawson *et al.*, 2008; Simmonds and MacLennan, 2005).

In addition to backscatter from micronekton, aggregative structures, or shoals, were selected by combining thresholded data from the two frequencies, then averaging them with a  $5 \times 5$  pixel smoothing matrix using ECHOVIEW software. The minimum threshold was set to  $-65$  dB at both frequencies. The smoothed averages were used to create a mask which was applied to the original 38-kHz echograms to extract the shoals (Simmonds and MacLennan, 2005).  $S_v$  from the shoals were integrated to obtain relative biomass estimates, NASC, over bins identical to those used for the scattering layer integrals. Since the sonic scattering layer is composed mostly of organisms undergoing diel vertical migration, daytime and nighttime backscatter from both the shallow scattering layer (SSL) and the deep scattering layer (DSL) had to be analyzed separately. Scrutinizing echograms revealed that transition times started after 5 am/pm and ended before 8 am/pm during crepuscular periods, which lasted from 05:56 to 06:40 and from 18:23 to 19:07,  $\pm 6$  min. As echograms revealed no noticeable vertical drift of organisms outside the 5 am/pm to 8 am/pm window, both the 38-kHz and the 120-kHz bioacoustic records were divided into daytime (08:00–17:00) and night

time (20:00–05:00) components to be examined separately.

### Statistical analyses

To examine spatial patterns in the datasets, multivariate analysis was carried out on the CTD and acoustics variables. As  $S_v$  is identical to  $\log_{10}(\text{NASC})$  times a constant, using it instead of NASC restored the required symmetry in the dataset.  $S_v$  was vertically normalized to be used as proxy for relative biomass. Using variograms, the autocorrelation in the datasets was determined to be negligible beyond 50 m vertically and 1 nmi horizontally (note that data from CTD casts showed no horizontal autocorrelation). Thus, center-scaled CTD variables (temperature, salinity, dissolved oxygen, and chlorophylls) and  $S_v$  were averaged into 50-m vertical bins.  $S_v$  was additionally averaged into 1-nmi horizontal bins to form 50 m  $\times$  1 nmi Elementary Sampling Units (ESUs). This procedure established the independence of each observation without losing important variability in the datasets. The number of aggregative structures, or shoals (NSHl for number of shoals), was also summed within each ESU. To simplify the datasets, principal components analyses (PCA) were used on the CTD and acoustic variables and the first two PCs retained. To divide the variables and observations into distinct groups with similar profiles, cluster analyses were carried out on the first two PCs using the hierarchical clustering method (Legendre and Legendre, 1998).

## RESULTS

### Physical properties and albacore CPUE

Weekly SLA maps show the eddy field characterized by relatively high temporal variability on scales

<1 week in the EEZ (not shown). During the 2-week period of this study the eddy field in the EEZ was dominated by anticyclonic eddies (Fig. 3) with a mean SLA SD of  $5.04 \pm 0.14$  cm, significantly higher than the  $4.20 \pm 0.12$  cm mean of the last 15 yrs (all confidence intervals are given at the 95% confidence level) (Fig. 2a). For 1992–2007, the strength of the SECC positively correlated with the number ( $r^2 = 0.67$ ,  $P = 0.009$ ) and strength ( $r^2 = 0.74$ ,  $P = 10^{-4}$ ) of anticyclonic eddies found in the EEZ.

During the last 15 yrs, exceptionally high SECC strengths and eddy activity in the EEZ during the peak months of March and April correspond to El Niño events (Fig. 2a). Of the six El Niño years, all but one were followed by high peaks in eddy activity in the EEZ. The best correlation between SOI and SLA SD in the EEZ ( $r^2 = 0.31$ ,  $P = 10^{-3}$ ) was obtained by lagging the SLA SD time-series 7 months relative to that of the SOI. Post-expansion albacore CPUE follows a similar trend. Peaks in SLA SD are followed by relatively high CPUEs, whereas during the year the SECC failed to intensify (2004), albacore CPUE showed a corresponding drop (Fig. 2a,b). Further, lagging monthly albacore CPUE by 8 months relative to the SOI time-series results in a correlation coefficient of  $r^2 = 0.35$ , significant at the 95% confidence level ( $P = 10^{-4}$ ). The 7-month SLA SD and 8-month albacore CPUE lag with SOI indicate that peaks in CPUE (April–June) lag behind those in SLA SD (March–May) by 1 month. Indeed, applying a 1-month lag to the CPUE time-series relative to those of the SLA SD results in a correlation coefficient that is significantly different from zero ( $r^2 = 0.34$ ,  $P = 10^{-4}$ ).

Monthly ocean color maps reveal seasonal and ENSO-scale variability in surface Chl *a*. During boreal winter months (December–February), Chl *a* concentrations peak at the north coast of New Guinea

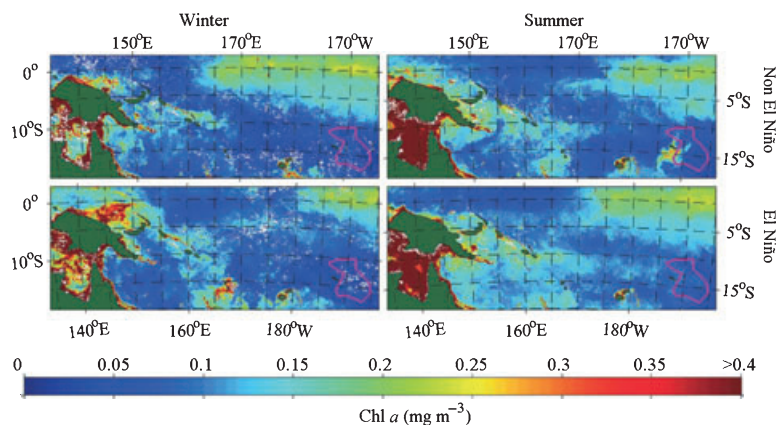


**Figure 4.** Representative monthly sea surface Chl *a* concentrations over the South-western Pacific in winter (left) and summer (right) during non El Niño (top) and El Niño (bottom) conditions. The borders of the American Samoa EEZ are shown at the lower right in magenta.

(Fig. 1), resulting in hypertrophic conditions ( $>1.00 \text{ mg m}^{-3}$ ), while in SECC waters Chl *a* concentrations are ultraoligotrophic ( $<0.06 \text{ mg m}^{-3}$ ) (e.g., Fig. 4, left panels) (classification was as defined by Shushkina *et al.* (1997):  $<0.06$  ultraoligotrophic,  $0.06\text{--}0.1$  oligotrophic,  $0.1\text{--}0.3$  mesotrophic,  $0.3\text{--}1.0$  eutrophic, and  $>1.0$  hypertrophic). Between April and July, Chl *a* concentrations at the north coast of New Guinea are ultraoligotrophic or mesotrophic ( $0.1\text{--}0.3 \text{ mg m}^{-3}$ ) and relatively high in the western SECC ( $0.15\text{--}0.20 \text{ mg m}^{-3}$ ), decreasing toward the east and extending typically to  $170^\circ\text{E} - 175^\circ\text{E}$  (e.g., Fig. 4, top right panel). During the winter months of El Niño years, hypertrophic conditions exist over a much larger region at the north coast of New Guinea and last for an extended time, starting as early as October and ending in April–May. The extended hypertrophic conditions are followed by an increase in Chl *a* concentrations in SECC waters, which now cover a markedly larger area and extend past the dateline (e.g., Fig. 4; compare upper and lower panels). In fact, during the last 10 yrs each El Niño event corresponds to relatively high Chl *a* concentrations at the north coast of New Guinea, which are followed by relatively high Chl *a* concentrations extending further east in the SECC than in other years.

During the 2 weeks of the *in situ* observations, the northern and southern halves of the American Samoa EEZ show distinct water characteristics as indicated by the CTD variables (Fig. 5). The northern half of the EEZ is characterized by a deep ( $>100 \text{ m}$ ) mixed layer, high near surface ( $0\text{--}50 \text{ m}$ ) temperatures ( $>29^\circ\text{C}$ ), high DO ( $>4.3 \text{ mL L}^{-1}$ ), high chloropigment concentrations ( $>0.02 \text{ mg m}^{-3}$ ), and low salinities

( $<34.7$ ) relative to those at the southern half ( $<29^\circ\text{C}$ ,  $< 4.3 \text{ mL L}^{-1}$ ,  $< 0.02 \text{ mg m}^{-3}$ , and  $>34.7$ , respectively). DO peaks between 100 and 200 m. Chloropigment concentrations peak between 100 and 150 m, generally higher in the northern part of the EEZ than in the southern part. At greater depths, between 500 and 1000 m (not pictured), the northern half of the EEZ shows higher salinities and lower dissolved oxygen than those at the southern half, with temperatures relatively stable overall.

To examine the effects of eddies associated with the  $\leq 200\text{-m}$ -deep SECC, averages of the four CTD variables in the upper 200 m were calculated to capture variability that is due mostly to eddy activity. Figure 6a shows that besides the north–south trend, the two northern and southern transects show differences in their water characteristics. The upper 200-m salinities are lowest at the Northwest Eddy, increase along Transect 1 with increasing distance from the eddy, and reach the highest values at Transect 2. Chloropigment concentrations are highest in the Northwest Eddy, then decline through Transect 1 and Transect 2. In fact, chloropigment concentrations are over a third higher at the Northwest Eddy than at the other northern transect (Transect 1), and salinities increase one and a half times from inside the eddy to the outside. At the southern part of the EEZ, the upper 200-m salinities are three-quarters higher at Transect 2 than at Transect 3, while average temperatures show a  $0.2^\circ\text{C}$  increase. Indeed, temperature and salinity at Transect 3 are similar to those at Transect 1.

These characteristic trends are reflected in the results of cluster analyses on the first two PC scores of the CTD variables, explaining 77% (66 and 11% for

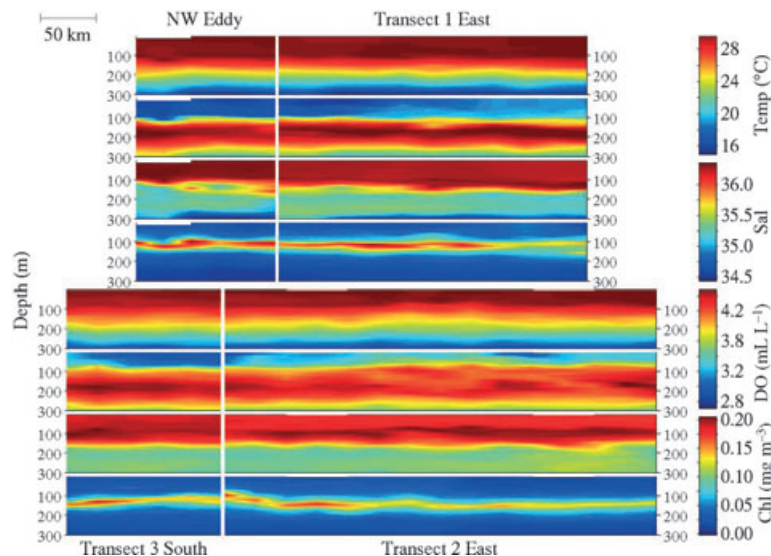
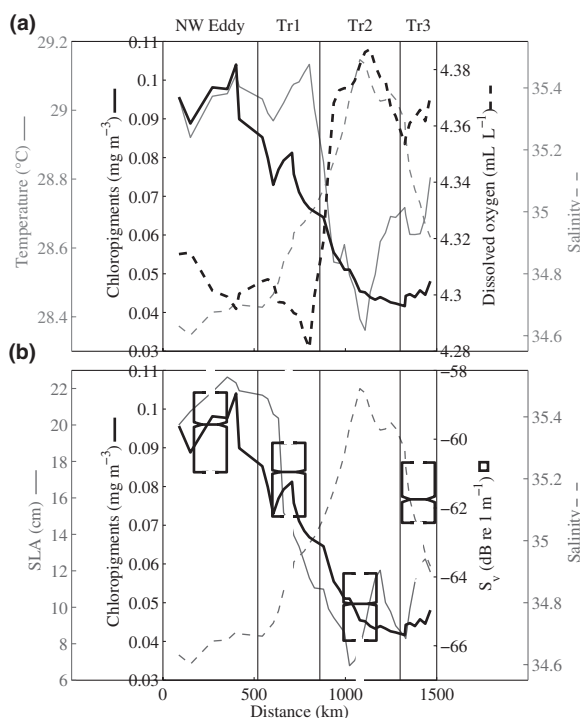


**Figure 5.** Upper 300-m CTD profiles for the northern (top) and southern (bottom) half of the EEZ. Each profile consists of four panels (from top): temperature, salinity, dissolved oxygen, and chloropigment concentrations, and are organized to correspond to the SLA maps in Fig. 3. Distances shown are as calculated between CTD casts.

**Figure 6.** Physical and biological characteristics at the four study sites with available CTD data, separated by the vertical lines. Distances shown are as calculated along ship tracks. (a) Upper 200-m CTD variables and (b) relative biomass (nighttime mean 38-kHz  $S_v$  in the upper 1000 m) with SLA and upper 200-m chloropigment concentrations and salinity. Boxes in the  $S_v$  boxplot represent the first, second, and third quartile of the medians, with notches indicating the 95% confidence intervals (Chambers *et al.*, 1983).



the first and second PC, respectively) of the variability. Clustering the CTD variables into two clusters separates the transects in the northern part of the EEZ from those in the southern part (Fig. 7a). Further clustering the first two PC scores into four clusters separates the Northwest Eddy from Transect 1, and Transect 2 from Transect 3 (Fig. 7b).

*In situ* measurement of currents in the EEZ show relatively high spatial (Fig. 8a) and temporal variability (e.g., Fig. 8b). On average, current magnitudes are  $9.46 \pm 0.28 \text{ cm s}^{-1}$  in the upper 200 m, strongest near the surface and between 100 and 200 m. The highest upper 200-m current values ( $\sim 20\text{--}25 \text{ cm s}^{-1}$ ) are observed near the Island of Tutuila,  $\sim 170^\circ 45' \text{W}$ ,  $14^\circ 15' \text{S}$  (Fig. 8a). This increase is a result of a strong, subsurface zonal jet between 100 and 200 m depth, with velocities exceeding  $40 \text{ cm s}^{-1}$  (e.g., Fig. 9) and directions to the west–southwest (Fig. 8a). At depth, between 500 and 700 m, current magnitudes are lower than in the upper 200 m, with a mean of

$6.39 \pm 0.20 \text{ cm s}^{-1}$  for the entire cruise, and peaking along Transect 1 to Transect 2 (Table 1). Mean current directions in the upper 200 m do not show a dominant trend, while below 500 m, north of  $12^\circ \text{S}$  the predominant current directions are to the east and south of  $12^\circ \text{S}$  they are mostly to the west.

#### Characteristics of albacore forage

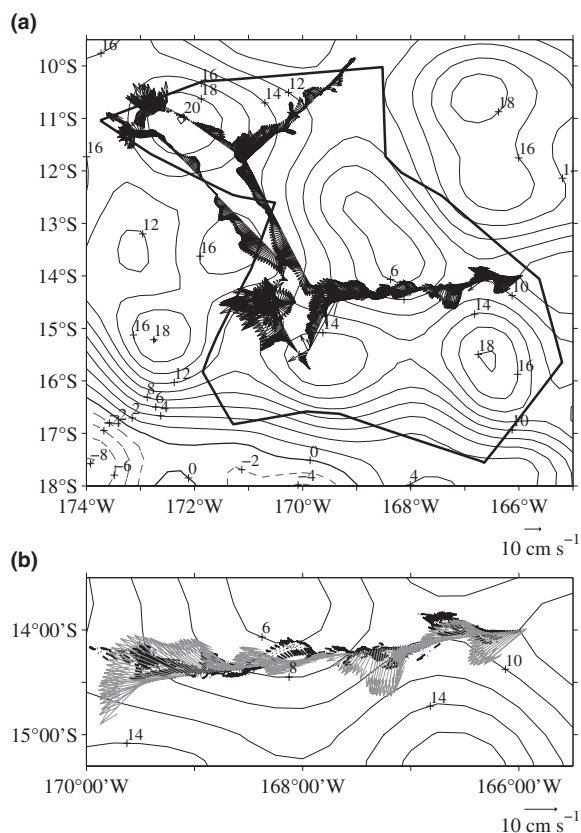
*In situ* acoustic backscatter data obtained within the American Samoa EEZ reveal the dynamic nature of the scattering layers (e.g., Fig. 10). The SSL extends to about 200–220 m in depth, prominent only during nighttime. In general, density of the SSL increases from daytime to nighttime (Table 2a). The more pronounced diel change at the lower frequency results in an overall 7.3-dB decrease in  $\delta S_v$  from day to night (Table 2a). The DSL is observed between 500-m and 900-m depths, consisting of two dominant layers: the ‘shallow’ DSL, between 500 and 650 m, and the ‘deep’ DSL, between 700 and 900 m (e.g., Fig. 10). It is evident from Fig. 10 that some organisms migrate between the deep DSL and the SSL, whereas others move between the shallow DSL and the SSL during transition times.

In contrast to the diel nature of the SSL, the DSL is more of a permanent layer, with diel density and biomass changes 1/4 and 1/10 of those of the SSL, respectively (Table 2a,b and Figs 10 and 11). The largest diel changes in biomass occur in the upper 80 m, with a more modest change between 80-m and 220-m depths (Fig. 11 left panel). Nighttime relative biomass at Transect 2 is about a third lower than at all other regions (Table 2c), with the DSL exhibiting a prominent diel change (compare left and right panels in Fig. 11). These differences result in a marked difference between the vertical structure of the backscatter at Transect 2 and the rest of the regions. Relative biomass does not change from day to night between 450 and 500 m, with most of the diel pattern in the DSL being seen between 500 and 700 m and between 750 and 850 m at Transect 2 and between 525 and 600 m and between 700 and 850 m at all other regions.

Although the diel changes are more prominent in the SSL than in the DSL, the SSL remains significantly denser even during daytime, with  $P < 10^{-6}$  (Table 2a). However, SSL densities measured at the two frequencies are only significantly different from each other during nighttime. In contrast to densities, the relative biomass of the DSL exceeds that of the SSL during daytime as a result of its larger vertical extent (Table 2b). Between the SSL and DSL, typically between 175- and 300-m depths, a thin, permanent layer of organisms was observed. Relative



**Figure 8.** Upper 200-m current magnitudes and directions (a) in the American Samoa EEZ for the entire cruise and (b) over Transect 2 East (black) and West (gray). Minimum and maximum times between observations at the same location along Transect 2 are a few minutes (east end) and 2.5–3.5 days (west end). Gray dashed and solid black contours show negative and positive SLA, respectively, with the thick black contour indicating the zero line. Decreasing and increasing SLA towards eddy cores are indicative of cyclonic (clockwise) and anticyclonic (anticlockwise) flow (see Fig. 3).



shoals, as well as the highest number of shoals of all regions within the EEZ (Table 2c). Shoals do not show a diel pattern in their vertical distribution. All shoals were found exclusively in the upper 400 m, with most observations occurring between 150 and 300 m (Fig. 11). Densities of shoals were significantly higher than those of micronekton (Table 2a), with  $\delta S_v$  between  $-2.0$  and  $-0.5$  dB. The majority of shoals shallower than 150 m were recorded at Transect 2, with almost all shoals observed only during daytime. In all other regions, aggregative structures were found in a narrower vertical band relative to those at Transect 2, centering on 200 m. At these locations, nighttime observations exceeded those of the daytime.

Including regions where hydrographic data are unavailable, two sites, the Test Site and Transect 3

North (Table 1), show the highest relative biomass of all regions ( $1200$  and  $1000 \text{ m}^2 \text{ nmi}^{-2}$ , respectively), exceeding those at the Northwest Eddy ( $900 \text{ m}^2 \text{ nmi}^{-2}$ ). These two sites are located immediately south of Tutuila, the main island of American Samoa (Fig. 3), where the highest magnitude upper 200-m currents were observed (Fig. 8a).

Cluster analysis on the first two PCs of  $S_v$  and NSHl, explaining 61.8% of variability in the dataset (50.7 and 11.1% for the first and second PC, respectively), confirms the main characteristics in the vertical structure of the scattering layer and the distinct nature of the aggregative structures (Fig. 7c). Clustering the first two PC coefficients into five clusters clearly separates the SSL, including the persistent 175–300-m layer (cluster 1, upper 400 m), the shallow DSL (cluster 2, 400–600 m), the area between the shallow and deep DSL (cluster 3, 600–700 m), and the deep DSL and below (cluster 4, 700–1000 m). NSHl forms one separate cluster (cluster 5), as its vertical structure does not correspond with those of the scattering layers. The distinct biological characteristics of Transect 2 are confirmed by the results of cluster analysis on the first two PC scores of the  $S_v$ /NSHl data. Clustering the first two PC scores into two clusters shows the separation of Transect 2 (cluster 1) from all the other transects (cluster 2) within the American Samoa EEZ (Fig. 7d).

## DISCUSSION

### Water masses in the EEZ

Data from the CTD cast reveal the presence of water masses in the EEZ that are carried by the SEC and by the SECC. Upper 200-m salinities ( $<35$ ) and temperatures ( $\geq 29$ ) in the Northwest Eddy and Transect 1 (Fig. 6a) are characteristics of waters in the Pacific warm pool and below the South Pacific Convergence Zone (SPCZ) (e.g., Levitus, 1982; Tomczak and Godfrey, 1994; Reid, 1997; Webb, 2000). The SECC originates east of New Guinea in the warm pool (Qu and Lindstrom, 2002) and follows the SPCZ to the vicinity of the American Samoa EEZ (Fig. 1a). Consequently, it carries high-temperature and low-salinity waters from the warm pool to the east and across the northern part of the American Samoa EEZ.

Near-surface higher salinities ( $>35$ ) and lower dissolved oxygen concentrations ( $<4.3 \text{ mL L}^{-1}$ ) in the south compared to the north (Fig. 5) represent South Pacific Eastern Subtropical Mode Waters (SPESMW – see Fig. 1b), near-surface subtropical gyre waters carried from the east by the SEC (Qu and Lindstrom,

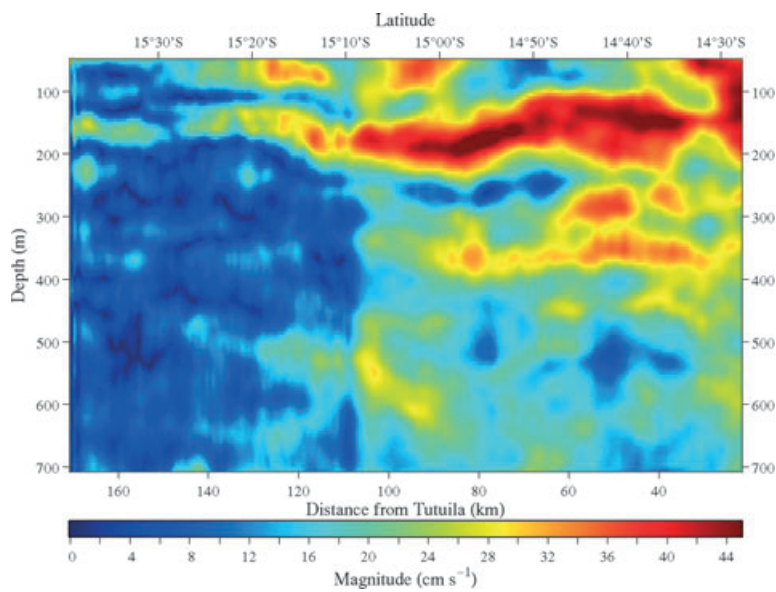


**Figure 9.** Current magnitudes along Transect 3 North (for the location of this transect, see Table 1 and Fig. 3, lower left panel). Direction of currents is to the southwest, as shown in Fig. 8a.

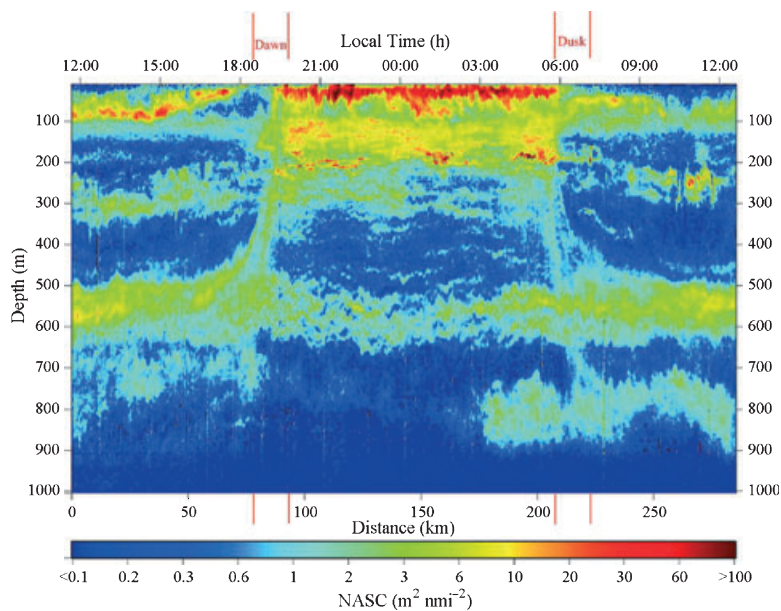


**Figure 10.** Typical 24-h pattern of the scattering layers at the 38-kHz frequency, taken from Transect 1 West.

2002). Note that the DO maxima at around 100 m depth are responsible for the higher upper 200 m average DO in the south relative to the north (Fig. 6a). The salinity maximum at  $\sim 170$ – $220$  m in both north and south (Fig. 5) is the signature of waters carried by the SEC in its core, which are formed in the windy, dry center of the southeast Pacific gyre (Hanawa and Talley, 2001). It follows that the approximate depth of 200 m marks the vertical extent of the SECC (Fig. 1b), corresponding to expectations (Qu and Lindstrom, 2002).

Higher DO concentrations in the south relative to the north between  $\sim 200$  and  $350$  m (Fig. 5) are characteristic of the South Pacific Tropical Water (SPTW) of the SEC (Fig. 1b), with DO concentrations of  $\sim 3.6$  and  $\sim 3.5$   $\text{mL L}^{-1}$  at around  $5$ – $12^\circ$  and  $12$ – $20^\circ\text{S}$ , respectively (Qu and Lindstrom, 2002). Below 400 m, relatively high DO south of  $12^\circ\text{S}$  is characteristic of the Antarctic Intermediate Water (AAIW), which is formed in the southeast Pacific and carried west by the deep extension of the SEC (Qu and Lindstrom, 2002). To the north, SEC waters are

**Table 2.** Mean (a) relative density ( $S_v$ ) and (b) relative biomass (NASC) of the SSL (15–220 m), DSL (500–900 m), ‘thin layer’ (175–300 m), and shoals during daytime and nighttime, and (c) at Transect 2 versus the rest of the transects.  $\delta S_v$  (relative composition) of the SSL and thin Layer are also included in (a) and (c), with shoal  $\delta S_v$  in (a) and NShl in (c).

	SSL (dB)		DSL (dB)		Thin layer (dB)		Shoal (dB)	
	38 kHz	120 kHz	38 kHz	120 kHz	38 kHz	120 kHz	38 kHz	120 kHz
(a)	$\delta S_v$	$\delta S_v$	$\delta S_v$	$\delta S_v$	$\delta S_v$	$\delta S_v$	$\delta S_v$	$\delta S_v$
Day	$-61.6 \pm 0.4$	$-61.1 \pm 0.5$	$-62.6 \pm 0.5$	$-61.6 \pm 0.6$	$-62.5 \pm 0.5$	$-61.6 \pm 0.6$	$-49.9 \pm 0.7$	$-52.0 \pm 0.8$
Night	$-52.5 \pm 1.2$	$-55.7 \pm 1.1$	$-64.6 \pm 0.8$	$-62.8 \pm 1.3$	$-60.4 \pm 1.1$	$-62.8 \pm 1.3$	$-50.0 \pm 0.6$	$-51.1 \pm 0.5$
Diel change	$8.6 \pm 1.6$	$5.4 \pm 1.9$	$2.0 \pm 0.3$	$1.2 \pm 1.2$	$2.1 \pm 0.7$	$1.2 \pm 1.2$	$0.1 \pm 0.5$	$0.1 \pm 0.4$
(b)	SSL ( $\text{m}^2 \text{nmi}^{-2}$ )		DSL ( $\text{m}^2 \text{nmi}^{-2}$ )		Thin layer ( $\text{m}^2 \text{nmi}^{-2}$ )		Shoal ( $\text{m}^2 \text{nmi}^{-2}$ )	
	38 kHz	120 kHz	38 kHz	120 kHz	38 kHz	120 kHz	38 kHz	120 kHz
Day	$101 \pm 5$	$76 \pm 7$	$124 \pm 6$	$106 \pm 6$	$106 \pm 6$	$74 \pm 8$	$17 \pm 4$	$17 \pm 4$
Night	$495 \pm 11$	$209 \pm 9$	$92 \pm 4$	$161 \pm 5$	$161 \pm 5$	$77 \pm 6$	$32 \pm 5$	$32 \pm 5$
Diel change	$394 \pm 8$	$133 \pm 7$	$32 \pm 5$	$55 \pm 7$	$55 \pm 7$	$3 \pm 8$	$15 \pm 4$	$15 \pm 4$
(c)	Total NASC ( $\text{m}^2 \text{nmi}^{-2}$ )		Shoal NASC ( $\text{m}^2 \text{nmi}^{-2}$ )		SSL $\delta S_v$		Thin layer $\delta S_v$	
	231 $\pm$ 5	842 $\pm$ 8	139 $\pm$ 6	45 $\pm$ 3	Day (dB)	Night (dB)	Day (dB)	Night (dB)
Transect #2			$1.82 \pm 0.47$	$0.25 \pm 0.21$	$2.3 \pm 0.3$	$-2.0 \pm 0.3$	$1.9 \pm 0.2$	$-1.5 \pm 0.3$
All but Tr #2					$-0.2 \pm 0.1$	$-4.0 \pm 0.2$	$0.1 \pm 0.1$	$-3.2 \pm 0.1$

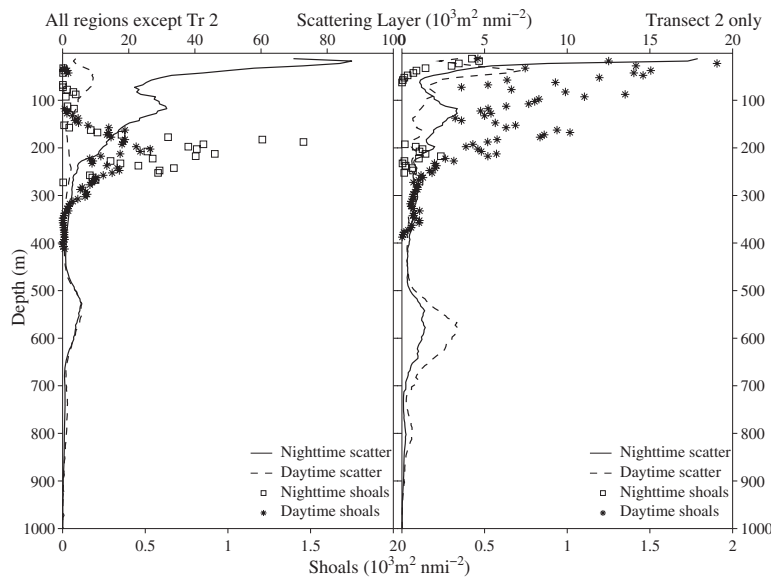


**Figure 11.** Vertical structure of the 38-kHz backscatter, with NASC values of shoals overlain for all regions except Transect 2 (left) and for Transect 2 only (right).

replaced by waters carried from the west by the eastward flowing ‘unnamed current’, observed by Qu and Lindstrom (2002) at 179°E between 12°S and 8°S, and between 15°S and 7°S at 500- and 1000-m depths, respectively (Fig. 1b). Current data from 400 m and below correspond with the westward and eastward direction of the SEC and the unnamed current, south and north of 12°S, respectively. The relatively high (low) DO in the southern (northern) part of the EEZ below 400 m is consistent with findings of Domokos *et al.* (2007), who observed the oxygen front at around 14°S, farther south than the present observations. The latitudinal difference in the DO front between the two studies is possibly the result of variability in the meridional position of the unnamed current, the deep extension of the SEC, or both.

#### Effects of the SECC in the EEZ

Areas occupied by SECC waters, predominantly the northern part of the EEZ, correspond to areas with relatively high chlorophyll concentrations and increased micronekton biomass (Fig. 6b). The origin of the higher productivity is most likely the result of seasonal upwelling at the north coast of New Guinea. During boreal winter (October–January), the northwesterly monsoon results in the reversal of the New Guinea Coastal Current (NGCC – see Fig. 1a), which exceeds 100 cm s<sup>-1</sup> magnitude eastwards. Eastward flow in the NGCC results in coastal upwelling (Kuroda, 2000), followed by the observed enhanced primary productivity in December–February (Fig. 4, left panels). Most of the eastward flow in the NGCC feeds the SECC (Qu and Lindstrom, 2002), which

peaks in strength a few months later and carries waters with high Chl *a* concentrations farther east (e.g., right panels of Fig. 4; also see Fig. 1a). Enhanced primary productivity in the NGCC and SECC presumably results in enhanced secondary production, thus providing food for micronekton and allowing for the observed increase in their biomass in the EEZ. The increasing zooplankton and micronekton biomass as the SECC propagates east likely deplete Chl *a* concentrations in time, which results in the oligotrophic conditions (0.06–0.10 Chl *a* mg m<sup>-3</sup>) east of ~170°–180°E (Fig. 4, right panels). However, note that since micronekton is observed to be vertically migrating from as deep as 900 m, deep currents and water characteristics might also play a role in their distribution. It follows then that the difference in micronekton biomass between areas north and south of 12°S could also be partially the result of the differences in water characteristics of the AAIW in the SEC and the water mass in the unnamed current.

Higher micronekton biomass in SECC waters in the EEZ suggests higher biomass of albacore in the presence of prey. Albacore biomass in the South Pacific is shown to be heavily influenced by the availability of prey (e.g., Josse *et al.*, 1998; Bertrand *et al.*, 2002a,b; Domokos *et al.*, 2007), whereas environmental factors are found not to affect albacore distribution and catchability in the American Samoa EEZ (Domokos *et al.*, 2007). Thus, seasonal increase in albacore biomass in SECC waters is consistent with the seasonally increased albacore CPUE rates observed by Domokos *et al.* (2007) in the northern half of the EEZ for the years of 2002–2003. In addition, the yearly

time-series of peak-month albacore CPUE corresponds directly to eddy activity in the EEZ for the 6-yr period of 2002–2007 (Fig. 2b).

The timing of the primary productivity bloom in the NGCC, the peak in the strength of the SECC, and the increase in albacore CPUE rates provide further support for the argument that the increase in primary productivity is responsible for the observed increase in micronekton biomass, which, in turn, results in an increase in albacore biomass and its CPUE. The north coast of New Guinea lies more than 5000 km to the west-northwest of the EEZ (Fig. 1a), a distance that the slow-flowing SECC, with a maximum mean flow of  $\leq 10 \text{ cm s}^{-1}$  (Qiu and Chen, 2004), takes at least 3 months to traverse. An approximate 3-month time frame corresponds with the lag between the December–February peak in hypertrophic conditions in the NGCC and the observed March–May peak in eddy activity in the EEZ. This time would allow for the development of higher micronekton biomass along the way and for the depletion of high primary production by the organisms it supports. The arrival of micronekton-rich waters at the EEZ in March–May coincides with the timing of the increase in albacore CPUE, observed for the months of April–June in 2002–2007. Note that instead of the observed 1-month lag using the 2002–2007 time series, Domokos *et al.* (2007) found a 2-month lag using the 3-yr record of 2002–2004.

Differences in micronekton composition in SECC and SEC waters (Table 2c) support their distinct origin. Although some micronekton could be advected into the convergent SECC as it travels to the EEZ, significant advection is not supported by the results of this study. As the SECC is surrounded by SEC waters arriving from the vicinity of the EEZ (Fig. 1a), substantial advection would eliminate the observed significant differences in micronekton composition between the SECC and SEC.

#### *Characteristics of eddies and their effects in the EEZ*

Besides the large-scale temporal and spatial effects of the SECC in the EEZ, mesoscale variability seems to play an important role. Observed similarities in the upper 200-m current directions and the expected geostrophic flow from SLA (Fig. 8) suggest a dominant geostrophic component during the time of the study; i.e., near-surface waters are characterized by the predominantly anticyclonic eddy field. The dominance of eddy kinetic energy over that of the current flow is a characteristic feature of the SECC. Qiu and Chen (2004) showed that the mean eddy kinetic energy associated with the SECC is equivalent to a  $15 \text{ cm s}^{-1}$

root mean square velocity anomaly which is higher than the  $\leq 10 \text{ cm s}^{-1}$  mean flow. Although far from the strong intensification observed in years such as 2003 or 2005, during the 2-week period of this study the eddy activity was significantly higher than that of the mean (Fig. 2a) and corresponded with the positive correlation found between the strength of the SECC and the strength and number of the resulting eddy activity in the EEZ.

The relatively stable and strong Northwest Eddy has a positive effect on both primary productivity and micronekton biomass, as indicated by its elevated Chl *a* concentrations and depth-normalized  $S_v$  (Fig. 6b). These findings are consistent with a study of mid-ocean eddies associated with jets in oligotrophic regions, such as the ones in the American Samoa EEZ (Lima *et al.*, 2002). Using food-web models incorporated into an eddy-resolving general circulation model, Lima *et al.* showed that biomass accumulated at convergent mesoscale regions. Advection of micronekton into the Northwest Eddy from neighboring waters is further supported by the similarity in micronekton composition at the Northwest Eddy and at other SECC sites. Note that although Transect 3 shows temperatures and salinities consistent with those of SECC waters (Fig. 6a), its DO is more representative of SEC waters. The lack of intensification of productivity is not surprising based on the weak, transient nature of this eddy, showing indications of the presence of SEC waters advected in from nearby.

In contrast to the present observations, during the 2004 study of Domokos *et al.* (2007), eddy activity was significantly lower than the mean of the last 15 yrs ( $3.55 \pm 0.08$  versus  $4.20 \pm 0.12 \text{ cm}$ ; Fig. 2a). Eddies were predominantly cyclonic with no effect on primary productivity, whereas water characteristics were those of the SEC (see their Figs 1 and 5). It follows that the lack of seasonal intensification of the SECC and the resulting absence of SECC waters are the reasons that Domokos *et al.* failed to find correlation between eddy activity and micronekton biomass. The unusually low eddy activity is consistent with the lack of these eddies on primary productivity and mixed-layer depth, even though Lima *et al.* (2002) found primary production occurring in divergent cyclonic regions of mid-ocean eddies in oligotrophic waters. Low micronekton biomass during 2004 is consistent with low albacore CPUE (Fig. 2b), presumably in response to low biomass of albacore in the absence of prey.

The lack of agreement between the effects of eddies in the EEZ and those of most frontal or boundary current eddies, where, with the exception of very few studies (e.g., Weimerskitch *et al.* 2004; Ménard *et al.*

2005) micronekton biomass increases in cyclonic eddy centers and high-shear regions of eddy edges (e.g., Brandt, 1981; Fiedler and Bernard, 1987; Wiebe and Joyce, 1992; Seki *et al.*, 2002; Sassa *et al.*, 2002), is not surprising based on fundamental differences between those eddies and mid-ocean eddies. In contrast to those studies, the Lima *et al.* (2002) model did not produce increased biomass at high-shear regions of mid-ocean eddies. Further, the high NShl found at relatively high-shear regions of eddy edges at Transect 2 (Fig. 8b) is seemingly consistent with prior observations (Ménard *et al.*, 2005). However, the results of this study do not support that the highest (lowest) biomass of shoals (micronekton) are the result of high shear at eddy boundaries, as relatively high-shear regions in different parts of the EEZ (Fig. 8a) are not associated with low micronekton biomass or high NShl. It is likely that low micronekton biomass and high NShl are characteristics of SEC waters, as water characteristics at Transect 2 are the most consistent with those of the SEC.

Consistent with the 2004 observations, the thermocline does not shoal from the Northwest Eddy and along Transect 1 as expected (Fig. 5), whereas the presence of the eddy is confirmed by the *in situ* current records (Fig. 8a). This apparent lack of effect on the thermocline could be due to a large-scale downward slope in isotherms towards the equator in the upper 200 m, shown by Kessler and Gourdeau (2007) and observed previously by Domokos *et al.* (2007), which could cancel out the expected slope along Transect 1. However, the observed deeper mixed layers associated with SECC waters are consistent with expectations based on their higher SLA, associated with convergence and downwelling, and lower near-surface densities than those of the SEC. Lower densities are the results of similar near-surface temperatures but lower salinities in the SECC, characteristics that inhibit vertical mixing.

#### *Micronekton characteristics*

The results of this study indicate that the composition, relative biomass, aggregative characteristics, and vertical structure of micronekton in SECC waters are different than in SEC waters. Vertical migration was observed between the SSL and as deep as 900 m. The pronounced diel change in SSL biomass in combination with a much more subtle change in DSL biomass and the fact that the relative biomass of the nighttime SSL is about four times higher than that of the daytime DSL are consistent with the hypothesis that organisms might be migrating between the SSL and DSL to depths below 900 m.

The generally lower nighttime  $\delta S_v$  in the SSL relative to those during the day indicate that organisms with  $\delta S_v < 0$ , such as fish with gas bladders, gelatinous organisms with gas inclusions, and possibly squid (e.g., Simmonds and MacLennan, 2005; Goss *et al.*, 2001, 1998), make up the majority of migratory organisms. Micronekton trawl samples conducted in the area of the Northwest Eddy during the time of the acoustic recordings (Domokos, unpublished data) show higher proportions of fish and lower proportions of crustaceans (mostly shrimp-like organisms) in the nighttime SSL than in the daytime DSL. Nighttime DSL has the highest proportions of fish in the net samples, with species compositions that are not seen in the daytime DSL or in the SSL. These results add support to the likely vertical migration of organisms from and to below the DSL.

Note that the very low relative biomass of the DSL at Transect 2 could include a small low bias due to the observed highest  $\delta S_v$  values in the nighttime SSL at this location. High  $\delta S_v$  values indicate relatively low numbers of organisms that scatter more strongly at the lower frequency, such as fish, gelatinous organisms with gas inclusions, and possibly squid (e.g., Simmonds and MacLennan, 2005; Goss *et al.*, 2001, 1998), which compose the majority of vertically migrating organisms. As these organisms make up less of the SSL at Transect 2 than in other regions, it is likely that the composition of the DSL at Transect 2 is different from that at the other regions, somewhat decreasing the apparent biomass measured with 38 kHz at depth.

The permanent thin layer, associated with albacore tuna in the American Samoa EEZ (Domokos *et al.*, 2007) and in the French Polynesian EEZ (e.g., Josse *et al.*, 1998; Bertrand *et al.*, 2002a,b), has relatively constant  $\delta S_v$  at depths of 200 and 175 m during days and nights, respectively. These depths correspond to those at which tagged albacore spent most of their time in the EEZ (Domokos *et al.*, 2007). These relatively constant  $\delta S_v$  are lower than daytime SSL values but higher than those of nighttime, possibly indicating the composition of albacore's preferred prey.

The majority of shoals observed during this study are most likely composed of small pelagic fish, as indicated by their  $\delta S_v$  (Simmonds and MacLennan, 2005). Note that the number of shoals detected can be biased by the presence of a thick SSL (present in all regions but Transect 2), thereby introducing a low bias during nighttime when the SSL is prominent. As densities of shoals are significantly higher than densities of the nighttime SSL (Table 2a), this bias is unlikely to be significant in the present dataset.

### *El Niño influences*

The results of this study show a statistically significant positive relationship between El Niños, the resulting interannual variability in the strength of – predominantly anticyclonic – eddy activity, and albacore CPUE in the EEZ. During post-expansion years, each El Niño event was followed by exceptionally high intensification of eddy activity and albacore CPUE, while during 2004, a La Niña year when the SECC failed to intensify due to negative wind stress curl anomaly and SLA (Li and Clarke, 2007), albacore CPUEs are the lowest on record. Because the best correlation between interannual variability in the SECC and the occurrence of El Niños is with a 7-month lag, and SOI on average precedes the occurrence of El Niños by 4 months, eddy activity in the EEZ peaks after about 3 months of an El Niño event. Given that it takes 3 months for waters in the NGCC to reach the EEZ via the SECC during times when the SECC is at its strongest, the observed 3-month lag between El Niños and SLA SD in the EEZ supports the connection between the effects of ENSO at New Guinea, the interannual variability in the SECC, and the eddy activity in the EEZ.

The reason for increased micronekton biomass in SECC waters during El Niños is presumably the exceptionally strong anomalous wind bursts and eastward NGCC velocities which result in stronger upwelling and primary productivity at the north coast of New Guinea in El Niños than in the boreal winters of other years (e.g., Fig. 4, bottom left panel). Further, increased wind stress over the warm pool (Vialard and Delecluse, 1998) results in the dissipation and eastward deflection of the barrier layer (that is, the haline stratification; see Lukas and Lindström, 1991), allowing for vertical mixing and for an increase in primary productivity. As an example, Lehodey (2001) calculated Chl *a* concentrations at the NGCC and the Pacific warm pool for the 1982–1983 and 1997–2000 ENSO events using CZCS (coastal zone color scanner on board Nimbus-7 Satellite, operating from October 1978 to June 1986) and SeaWiFS satellite data and showed an exceptional increase in Chl *a* concentrations from ultraoligotrophic to hypertrophic and mesotrophic at the NGCC and warm pool, respectively. These prior findings correspond to the change in Chl *a* concentrations observed at the NGCC and over the warm pool during the El Niño events of the last decade (1998–2007) (e.g., Fig. 4).

Using a spatial environmental population dynamics model, Lehodey (2001) showed that the increased primary productivity leads to enhanced zooplankton

and micronekton biomass, primarily at the north coast of New Guinea, beginning at the peak of an El Niño event (highest negative SOI) and lasting for about 6 months. Results of this study show that the increased Chl *a* concentrations in waters of the NGCC and the warm pool during El Niño events are carried on by the exceptionally strong SECC and mesotrophic waters reach as far east as 175°W (e.g., Fig. 4, bottom right panel). Exceptional increase in Chl *a* is expected to result in an increase in micronekton biomass during the 3 months before waters in the SECC reach the EEZ, and presumably a proportional increase in albacore biomass due to the presence of prey.

The effects of ENSO on the distribution and biomass of tunas have been shown in previous studies. One such work documented the favorable effects of El Niño on the distribution and biomass of skipjack tuna in the western equatorial Pacific in response to the dissipation of the barrier layer and eastward shift of the warm-pool/coldtongue convergence zone, resulting in shifting favorable skipjack habitat eastward and an increase in micronekton biomass (Lehodey *et al.*, 1997, 1998; Lehodey, 2001). An eastward shift in preferred habitat for bigeye tuna during the 1997–1998 El Niño was considered a likely reason for increased bigeye CPUEs at Palmyra, although a possible vertical shift in the preferred habitat for bigeye and longline settling depths may have increased catchability (Howell and Kobayashi, 2006). Further, Polovina *et al.* (2001) hypothesized that increased albacore catch at the Transition Zone Chlorophyll Front (TZCF) during the 1997–1998 El Niño was the result of enhanced convergence at the TZCF, effectively concentrating albacore forage and increasing albacore catchability.

### *Local effects*

The strong ( $40+ \text{ cm s}^{-1}$ ) west-southwest flowing zonal jet at  $\sim 100\text{--}200$  m depth is likely the reason for the observed increase in micronekton biomass near and south of the Island of Tutuila (Figs 8a and 9), with no increase in Chl *a* (Fig. 6b). Strong subsurface zonal jets created by the interaction of the westward-flowing SEC and island-related topography have been observed in other regions such as New Caledonia, Vanuatu, and Fiji (e.g., Stanton *et al.*, 2001; Webb, 2000). Convergent waters associated with the topographically induced subsurface jet are expected to advect organisms such as micronekton into these regions from neighboring waters. Accumulation of organisms from plankton to micronekton and top predators have been previously documented at

convergent regions associated with increased flow at island edges (e.g., Johannes, 1981; Bakun, 2006). Further, eutrophic to hypertrophic conditions are present at various islands in the South-west Pacific, probably the results of upwelling due to island effects. For example, eutrophic to hypertrophic conditions are almost always present in the near vicinity of Fiji (Fig. 4, approximately at 177°E and 17°S), which blocks a strong band of the SEC and is responsible for the formation of two strong subsurface westward-flowing zonal jets, the North and South Fiji Currents (Webb, 2000).

Local, island-induced upwelling is likely the cause of the record CPUE in 2002, (Fig. 2b), a year with no El Niño event. That year corresponds to anomalous eutrophic conditions immediately south of Tutuila (Fig. 4, top right panel), which are likely the effect of anomalous upwelling caused by interactions between the observed subsurface jet and topography, probably due to changes in the magnitude and/or direction of the subsurface jet. Eutrophic conditions likely led to a pronounced increase in micronekton biomass and the observed high albacore CPUE during that year.

## CONCLUSION

This study provides evidence for the importance of the seasonal and ENSO-scale variability in the strength of the SECC and its associated anticyclonic eddies in the American Samoa EEZ. This variability positively affects micronekton biomass and CPUE of albacore in the EEZ, the target population of the local longline fishery. The results of this work show that during peak times, the enhanced SECC carries waters with high Chl *a* concentrations from upwelling regions of the north coast of New Guinea. SECC waters become oligotrophic by the time they reach the EEZ, mostly likely a result of the increasing biomass of zooplankton and micronekton as the SECC propagates east. The increased micronekton biomass in SECC waters is advected into relatively stable anticyclonic eddies and apparently concentrates the economically important albacore by providing forage, thus resulting in the observed increase in albacore CPUE. While the results of this study support the hypothesis that seasonal and climate-scale variability in the SECC impacts the distribution and/or biomass of albacore tuna, effectively linking the documented increase in primary productivity in SECC waters to that of micronekton biomass and of albacore CPUE, confirming these connections require further research. However, whether the increase in albacore CPUE is a result of an increase in their

biomass or an increase in their catchability, this study suggests that the strength of upwelling and the resulting increase in Chl *a* concentrations at the north coast of New Guinea and the SOI could be used to predict the performance and help in the management of the local longline fishery for albacore tuna in the American Samoa EEZ.

## ACKNOWLEDGEMENTS

The author wishes to acknowledge the help and support of many who made this project possible. I thank the officers and crew of the NOAA Ship, *Oscar Elton Sette*, as well as the scientific party for their work and dedication to the success of this study. I thank Jules Hummons for her help with processing the ADCP data and Mathieu Doray for statistical consultations. I thank Michael P. Seki and Jeffrey J. Polovina for obtaining funding for this work. I also wish to thank Jeffrey J. Polovina, Evan Howell, and Don Kobayashi for reading and providing helpful comments and/or instrumental suggestions on the draft of this manuscript. Further, I thank Deborah Yamaguchi for her help in creating the final version of the schematic in Fig. 1. This project was supported by the JIMAR Pelagic Fisheries Research Program of the University of Hawaii School of Ocean and Earth Science and Technology under Cooperative Agreement number NA17RJ12301 from the National Oceanic and Atmospheric Administration.

## REFERENCES

- Bakun, A. (2006) Fronts and eddies as key structures in the habitat of marine fish larvae: opportunity, adaptive response and competitive advantage. *Sci. Mar.* **70S2** 105–122.
- Bertrand, A., Le Borgne, R. and Josse, E. (1999) Acoustic characterization of micronekton distribution in French Polynesia. *Mar. Ecol. Prog. Ser.* **191**:127–140.
- Bertrand, A., Bard, F.X. and Josse, E. (2002a) Tuna food habits related to the micronekton distribution in French Polynesia. *Mar. Biology* **140**:1023–1037.
- Bertrand, A., Josse, E., Bach, P., Gros, P. and Dagorn, L. (2002b) Hydrological and trophic characteristics of tuna habitat: consequences of tuna distribution and longline catchability. *Can. J. Fish. Aquat. Sci.* **59**:1002–1013.
- Bigelow, K.A., Hampton, J. and Miyabe, N. (2002) Application of a habitat-based model to estimate effective longline fishing effort and relative abundance of Pacific bigeye tuna (*Thunnus obesus*). *Fish. Oceanogr.* **11**:143–155.
- Bigelow, K.A., Musyl, M.K., Poisson, F. and Kleiber, P. (2006) Pelagic longline gear depth and shoaling. *Fish. Research* **77**:173–183.
- Boggs, C.H. (1992) Depth, capture times, and hooked longevity of longline-caught pelagic fish: Timing bites of fish with chips. *Fish. Bull.*, U S **90**:642–658.

- Brandt, S.B. (1981) Effects of warm-core eddy on fish distributions in the Tasman Sea off East Australia. *Mar. Ecol. Prog. Ser.* **6**:19–33.
- Chambers, J.M., Cleveland, W.S., Kleiner, B. and Tukey, P.A. (1983) *Graphical Methods for Data Analysis*. Belmont: Wadsworth, P. 395.
- Cushing, D.H. (1982) *Climate and Fisheries*. London: Academic Press, P. 363.
- Domokos, R., Seki, M.P., Polovina, J.J. and Hawn, D.D. (2007) Oceanographic investigation of the American Samoa albacore (*Thunnus alalunga*) habitat and longline fishing grounds. *Fish. Oceanogr.* **16**:555–572.
- Fiedler, P.C. and Bernard, H.J. (1987) Tuna aggregation and feeding near fronts observed in satellite imagery. *Continental Shelf Res.* **7**:871–881.
- Goss, C., Middleton, D. and Rodhouse, P. (2001) Investigation of squid stocks using acoustic survey methods. *Fish. Res.* **54**:111–121.
- Goss, C., Rodhouse, P.G., Watkins, J.L. and Brierley, A.S. (1998) Identification of squid echoes in the south Atlantic. *CCAMLR Sci.* **5**:259–271.
- Graham, J.B., Lowell, W.R., Chin Lai, N. and Laurs, R.M. (1989) O<sub>2</sub> tension, swimming velocity, and thermal effects on the metabolic rate of the Pacific albacore, *Thunnus alalunga*. *Exp. Biol.* **48**:89–94.
- Hanawa, K. and Talley, L. (2001) Mode Waters. In: *Ocean Circulation and Climate Observing and Modelling the Global Ocean*. G. Siedler, J. Church & J. Gould (eds). San Diego: Academic Press, pp. 373–387.
- Holbrook, N.J. and Bindoff, N.L. (1997) Interannual and decadal temperature variability in the southwest Pacific Ocean between 1955 and 1988. *J. Climate* **10**:1035–1049.
- Howell, E.A. and Kobayashi, D.R. (2006) El Niño effects in the Palmyra Atoll region: oceanographic changes and bigeye tuna (*Thunnus obesus*) catch rate variability. *Fish. Oceanogr.* **15**:477–489.
- Jech, J.M. and Michaels, W.L. (2006) A multifrequency method to classify and evaluate fisheries acoustics data. *Can. J. Fish. Aquat. Sci.* **63**:2225–2235.
- Johannes, R.E. (1981) *Words of the Lagoon: Fishing and Marine Lore in the Palau District of Micronesia*. Berkeley: Univ. California Press, pp. xiv + 245.
- Josse, E., Bach, P. and Lagorn, L. (1998) Simultaneous observations of tuna movements and their prey by sonic tracking and acoustic surveys. *Hydrobiologia* **371/372**:61–69.
- Kessler, W. and Gourdeau, L. (2006) Wind-driven zonal jets in the South Pacific Ocean. *Geophys. Res. Lett.* **33**, L03608, doi:10.1029/2005GL025084.
- Kessler, W. and Gourdeau, L. (2007) The annual cycle of circulation of the southwest subtropical Pacific analyzed in an ocean GCM. *J. Phys. Oceanogr.* **37**:1610–1627.
- Kang, M., Furusawa, M. and Miyashita, K. (2002) Effective and accurate use of differences in mean volume backscattering strength to identify fish and plankton. *ICES J. Mar. Sci.* **59**:794–804.
- Kuroda, Y. (2000) Variability of Currents off the Northern Coast of New Guinea. *J. Oceanogr.* **56**:103.
- Langley, A.D. (2006) The south Pacific Albacore fishery: a summary of the status of the stock and fishery management issues of relevance to Pacific Island Countries and Territories. *Oceanic Fisheries Programme Technical Report No. 37*:viii + 26pp.
- Laurs, R.M. and Lynn, R.J. (1977) Seasonal migration of North Pacific albacore, *Thunnus alalunga*, into North American coastal waters: distribution, relative abundance and association with transition zone waters. *Fish. Bull. U S* **75**:795–822.
- Laurs, R.M., Fiedler, P.C. and Montgomery, D.R. (1984) Albacore tuna catch distributions relative to environmental features observed from satellites. *Deep-Sea Res.* **31**:1085–1099.
- Lavery, A.C., Wiebe, P.H., Stanton, T.K., Lawson, G.L., Benfield, M.C. and Copley, N. (2007) Determining dominant scatterers of sound in mixed zooplankton populations. *J. Acoust. Soc. Am.* **122**:3304–3326.
- Lawson, L.L., Wiebe, P.H., Stanton, T.K. and Ashjian, C.J. (2008) Euphausiid distribution along the Western Antarctic Peninsula; Part A: Development of robust multi-frequency acoustic techniques to identify aggregations and euphausiid size, abundance, and biomass. *Deep Sea Res. II.* **55**:412–431.
- Legendre, P. and Legendre, L. (1998) *Numerical Ecology*. Amsterdam: Elsevier, pp. 853.
- Lehodey, P. (2001) The pelagic ecosystem of the tropical Pacific Ocean: dynamic spatial modelling and biological consequences of ENSO. *Progr. Oceanogr.* **49**:439–468.
- Lehodey, P., Bertignac, M., Hampton, J., Lewis, A. and Picaut, J. (1997) El Niño Southern Oscillation and tuna in the western Pacific. *Nature* **389**:715–718.
- Lehodey, P., Andre, J.M., Bertignac, M., Hampton, J., Stoens, A., Menkes, C., Memery, L. and Grima, N. (1998) Predicting skipjack tuna forage distributions in the equatorial Pacific using a coupled dynamical bio-geochemical model. *Fish. Oceanogr.* **7**:317–325.
- Levitus, S. (1982) *Climatological Atlas of the World Ocean*. Princeton, NJ: NOAA ERL, GFDL Professional Paper, 13.
- Li, J. and Clarke, A.J. (2007) Interannual sea level variations in the south Pacific from 5° to 28°S. *J. Phys. Oceanogr.* **37**: doi:10.1175/2007JPO3656.1.
- Lima, I.D., Olson, D.B. and Doney, S.C. (2002) Biological response to frontal dynamics and mesoscale variability in oligotrophic environments: Biological production and community structure. *J. Geophys. Res.* **107**: doi:10.1029/2000JC000393.
- Lukas, R. and Lindström, E. (1991) The mixed layer of the western equatorial Pacific Ocean. *J. Geophys. Res.* **96**:3343–3457.
- MacLennan, D.N., Fernandes, P.G. and Dalen, J. (2002) A consistent approach to definitions and symbols in fisheries acoustics. *ICES J Mar Sci* **59**:365–369.
- Madureira, L.S.P., Ward, P. and Atkinson, A. (1993) Differences in backscattering strength determined at 120 and 38 kHz for three species of Antarctic macroplankton. *Mar. Ecol. Progress Series* **93**:17–24.
- Ménard, F., L'Évêque, J.J., Potier, M., Ternon, J.F., Baurand, F., Maury, O. and Marsac, F. (2005) Acoustic characterization of tropical tuna prey in the Western Indian Ocean in relation with local environmental conditions. *ICES C.M.* 2005/U:11, 13.
- Ménard, F., Marsac, F., Bellier, E. and Cazelles, B. (2007) Climatic oscillations and tuna catch rates in the Indian Ocean: a wavelet approach to time series analysis. *Fish. Oceanogr.* **16**:95–104.
- Polovina, J.J., Howell, E.A., Kobayashi, D.R. and Seki, M.P. (2001) The transition zone chlorophyll front, a dynamic global feature defining migration and forage habitat for marine resources. *Progr. Oceanogr.* **49**:469–483.

- Qiu, B. and Chen, S. (2004) Seasonal modulations in the eddy field of the South Pacific Ocean. *J. Phys. Oceanogr.* **34**:1515–1527.
- Qu, T. and Lindstrom, E.J. (2002) A climatological interpretation of the circulation in the Western South Pacific. *J. Phys. Oceanogr.* **32**:2492–2508.
- Reid, J.L. (1997) On the total geostrophic circulation of the Pacific Ocean: flow patterns, tracers, and transports. *Progr Oceanogr* **39**:263–325.
- Ressler, P.H., Brodeur, R.D., Peterson, W.T., Pierce, S.D., Vance, P.M., Røstad, A. and Barth, J.A. (2004) The spatial distribution of euphausiid aggregations in the Northern California Current during August 2000. *Deep-Sea Res. II*, Special Issue **52**:89–108.
- Ridgway, K.R., Godfrey, J.S., Meyers, G. and Bailey, R. (1993) Sea level response to the 1986–1987 El Niño–Southern event in the western Pacific in the vicinity of Papua New Guinea. *J. Geophys. Res.* **98**:16387–16395.
- Sassa, C., Kawaguchi, K., Kinoshita, T. and Watanabe, C. (2002) Assemblages of vertical migratory mesopelagic fish in the transitional region of the western North Pacific. *Fish. Oceanogr.* **11**:193–204.
- Seki, M.P., Lumpkin, R. and Flament, P. (2002) Hawaii cyclonic eddies and blue marlin catches: the case study of the 1995 Hawaiian International Billfish Tournament. *J. Oceanogr.* **58**:739–745.
- Simmonds, E.J. and MacLennan, D.N. (2005) *Fisheries Acoustics*. Oxford:Blackwell Science, pp. 431.
- Shushkina, E.A., Vinogradov, M.E., Lebedeva, L.P. and Anokhina, L.L. (1997) Productivity characteristics of epipelagic communities of the World's Oceans. *Oceanology* **37**:346–353.
- Stanton, B., Roemmich, D. and Kosro, M. (2001) A shallow zonal jet south of Fiji. *J. Phys. Oceanogr.* **31**:3127–3130.
- Tomczak, M. and Godfrey, J.S. (1994) *Regional Oceanography: An Introduction*. Oxford: Pergamon, x + 422pp.
- Vialard, J. and Delecluse, P. (1998) An OGCM study of the TOGA decade. Part I: role of salinity in the physics of the western Pacific fresh pool. *J. Phys. Oceanogr.* **28**:1071–1088.
- Walther, G.R., Post, E., Convey, P., et al. (2002) Ecological responses to recent climate change. *Nature* **416**:389–395.
- Ward, P. and Myers, R.A. (2005) Inferring the depth distribution of catchability for pelagic fishes and correcting for variations in the depth of longline fishing gear. *Can. J. Fish. Aquat.* **62**:1130–1142.
- Webb, D. (2000) Evidence for shallow zonal jets in the South Equatorial Current region of the southwest Pacific. *J. Phys. Oceanogr.* **30**:706–720.
- Weimerskirch, H., Le Corre, M., Jequemet, S., Potier, M. and Marsac, F. (2004) Foraging strategy of a top predator in tropical waters: great frigatebirds in the Mozambique Channel. *Mar. Ecol. Progr Ser.* **275**:297–308.
- Wiebe, P.H. and Joyce, T.M. (1992) Introduction of interdisciplinary studies of Kuroshio and Gulf Stream rings. *Deep Sea Res. I.* **39**:v–vi.